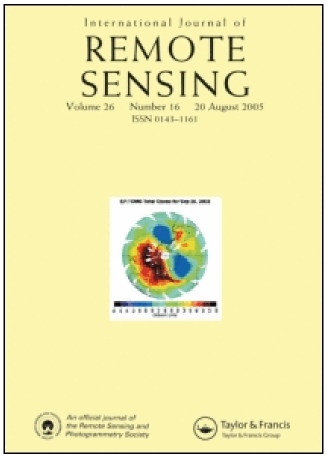

International Journal of Remote Sensing
Publication details, including instructions for authors and subscription information:
http://www.informaworld.com/smpp/title~content=t713722504

Atmospheric correction algorithm for MERIS above case-2 waters

To cite this Article: , 'Atmospheric correction algorithm for MERIS above case-2 waters', International Journal of Remote Sensing, 28:7, 1469 - 1486
To link to this article: DOI: 10.1080/01431160600962574
URL: http://dx.doi.org/10.1080/01431160600962574

International Journal of Remote Sensing
Vol. 28, No. 7, 10 April 2007, 1469–1486

Atmospheric correction algorithm for MERIS above case-2 waters

TH. SCHROEDER*†, I. BEHNERT‡§, M. SCHAALE†, J. FISCHER† and R. DOERFFER‡

†Free University Berlin, Institute for Space Sciences, Berlin, Germany
‡GKSS Research Centre, Institute for Coastal Research, Geesthacht, Germany
§CIMEL Electronique, Paris, France

(*Received 28 March 2006; in final form 5 June 2006*)

The development and validation of an atmospheric correction algorithm designed for the Medium Resolution Imaging Spectrometer (MERIS) with special emphasis on case-2 waters is described. The algorithm is based on inverse modelling of radiative transfer (RT) calculations using artificial neural network (ANN) techniques. The presented correction scheme is implemented as a direct inversion of spectral top-of-atmosphere (TOA) radiances into spectral remote sensing reflectances at the bottom-of-atmosphere (BOA), with additional output of the aerosol optical thickness (AOT) at four wavelengths for validation purposes. The inversion algorithm was applied to 13 MERIS Level1b data tracks of 2002–2003, covering the optically complex waters of the North and Baltic Sea region. A validation of the retrieved AOTs was performed with coincident *in situ* automatic sun–sky scanning radiometer measurements of the Aerosol Robotic Network (AERONET) from Helgoland Island located in the German Bight. The accuracy of the derived reflectances was validated with concurrent ship-borne reflectance measurements of the SIMBADA hand-held field radiometer. Compared to the MERIS Level2 standard reflectance product generated by the processor versions 3.55, 4.06 and 6.3, the results of the proposed algorithm show a significant improvement in accuracy, especially in the blue part of the spectrum, where the MERIS Level2 reflectances result in errors up to 122% compared to only 19% with the proposed algorithm. The overall mean errors within the spectral range of 412.5–708.75 nm are calculated to be 46.2% and 18.9% for the MERIS Level2 product and the presented algorithm, respectively.

1. Introduction

The high sensitivity and large dynamic range of the Medium Resolution Imaging Spectrometer (MERIS), operational since 2002 on board the European environmental satellite ENVISAT, enables accurate monitoring of the Earth's atmosphere and surface (Rast 1999). Special care was taken to obtain a sufficient signal-to-noise ratio above dark targets as found over open ocean waters in the near-infrared spectral region to perform an atmospheric correction with satisfactory precision. MERIS measures the reflected solar radiation in 15 programmable bands in the spectral range 412.5–900 nm with an average bandwidth of 10 nm. It is a nadir-looking push-broom imaging system with two spatial resolutions. Data are acquired in a full-resolution (FR) mode with 300 m on-ground resolution at the subsatellite

*Corresponding author. Email: Thomas.Schroeder@wew.fu-berlin.de

International Journal of Remote Sensing
ISSN 0143-1161 print/ISSN 1366-5901 online © 2007 Taylor & Francis
http://www.tandf.co.uk/journals
DOI: 10.1080/01431160600962574

point and in a reduced resolution (RR) mode with 1200 m on-ground resolution. The instrument consists of five identical cameras sharing a large field of view (68.5°), resulting in a swath of 1150 km. ENVISAT'S celestial orbit allows MERIS to cover the Earth's surface and atmosphere completely within 3 days. Thus the radiometric features as well as the short revisit time make MERIS one of the most important European orbiting instruments for remote sensing purposes (Rast 1999).

Atmospheric correction is one of the most limiting factors for an accurate retrieval of water constituents from satellite remote sensing data. A classification scheme of case-1 and case-2 water types was first introduced by Morel and Prieur (1977). In contrast to case-1 waters, in which the optical properties are determined solely by phytoplankton and associated constituents and the water itself, the spectral signatures of case-2 waters are also influenced by coloured dissolved organic matter and inorganic suspended particulate matter. In this optically complex water type, all water constituents can vary independently from each other. For both cases the accurate qualitative and quantitative retrieval from remotely sensed images requires removing the effects that result from scattering and absorption in the atmosphere and from reflection at the sea surface from the measured top-of-atmosphere (TOA) radiances. Such procedures are called atmospheric corrections. Without a carefully adapted atmospheric correction, reliable retrieval is not possible and multitemporal water quality studies based on satellite imagery would be biased by the influence of the highly variable atmosphere.

Standard atmospheric correction algorithms try to decouple the oceanic and the atmospheric signals from the total measured spectral information at the TOA. They assume the ocean colour to be black (complete absorption of incident radiation) in the near-infrared (NIR) spectral region (λ>700 nm) and therefore often fail above turbid case-2 waters because of the influence of highly scattering water constituents or bottom-up effects. Non-zero water-leaving radiances in the NIR will lead to an overestimation of the aerosol optical thickness (AOT) with the consequence of an over-correction in the visible (VIS) spectral region, which often results in negative water-leaving radiances.

Other, more suitable attempts to correct for the atmospheric influence above case-2 waters are based on iterative fitting approaches (Land and Haigh 1996) or on artificial neural network (ANN) techniques (Zhang *et al.* 2002, Zhang 2003, Jamet *et al.* 2004, Schroeder 2005). In another approach a simplified radiative transfer (RT) ocean–atmosphere model was used by Doerffer and Fischer (1994) within an optimization procedure for TOA reflectances of the Coastal Zone Colour Scanner (CZCS), which includes atmospheric correction as well as the retrieval of water constituents. The simple model was tuned for different angles by using the more exact results from the matrix-operator model (MOM).

2. Methodology: algorithm description

In contrast to standard approaches, the correction algorithm outlined here is not based on decoupling and takes into account not only the NIR spectral information but also the spectral signature of the VIS spectral region. The proposed algorithm uses the spectral information of 12 MERIS bands as compiled in table 1. The general methodology of the presented algorithm can be regarded as an integrated approach based on inverse modelling of RT calculations within a coupled ocean–atmosphere system by applying ANN techniques. Later on we give a detailed overview of the parameterization of the forward and the inverse models.

Table 1. Overview of all MERIS bands and those used by the proposed ANN-based atmospheric correction algorithm.

MERIS band	Centre wavelength (nm)	Bandwidth (nm)	Used by ANN algorithm
1	412.5	10	yes
2	442.5	10	yes
3	490	10	yes
4	510	10	yes
5	560	10	yes
6	620	10	yes
7	665	10	yes
8	681.25	7.5	no*
9	708.75	10	yes
10	753.75	7.5	yes
11	760.63	3.75	no†
12	778.75	15	yes
13	865	20	yes
14	885	10	yes
15	900	10	no‡

Reason for rejection: *chlorophyll fluorescence, †O_2-A absorption, ‡water vapour absorption.

2.1 *Forward model parameterization*

For the forward model we used an established and validated RT code based on the matrix-operator method, also known as adding-doubling (Fischer and Grassl 1984, Fell and Fischer 2001). The model simulates the light propagation through the ocean and the atmosphere and is used to generate a large data base of azimuthally resolved upward radiances in the MERIS channels just above the sea surface and at TOA for a variety of sun and observing geometries by taking varying amounts of different types of atmospheric and oceanic constituents into account.

All simulations were performed for a US standard atmosphere (NOAA, NASA, and USAF 1976) with a constant ozone loading of 344 Dobson units (DU). We considered a mixture of maritime and continental aerosol models according to Shettle and Fenn (1979) and the World Climate Research Program (WCRP 1986) for the boundary layer and the troposphere, while we assumed a constant loading of sulfuric acid (H_2SO_4) aerosols in the stratosphere (WCRP 1986), as outlined in table 2. The spectral aerosol extinction was modelled by five AOTs simulated in the range 0.03–1 at the reference wavelength of 550 nm. The optical properties of the aerosols used as input for the RT simulations were derived from Mie calculations and are shown in figure 1. In addition, a rough sea surface characterized by wind speeds of 1.5 and 7.2 $m\,s^{-1}$ according to a probability distribution function of wave facets of the Cox and Munk (1954) model and surface air pressure variations of 980 and 1040 hPa were considered. The ocean in the model is characterized by varying concentrations of water constituents typically found in European coastal waters, namely chlorophyll *a* (CHL), total (organic + inorganic) suspended matter (TSM) and yellow substance (YEL). Their concentration ranges covered in the simulations are 0.05–50 $mg\,m^{-3}$ for CHL, 0.05–50 $g\,m^{-3}$ for TSM and 0.005–1 m^{-1} (at 443 nm) for YEL. The inherent optical properties required as input to the RT simulations, such as the absorption and scattering coefficients of pure sea water, of CHL, TSM and YEL were taken from published measurements or parameterizations. The total absorption of the sea water (a_{WAT}) was modelled according to equation (1) as the sum of the absorption coefficients of pure sea water (a_w), the absorption of organic

Table 2. The eight aerosol models used for the proposed atmospheric correction algorithm. (A mixing ratio of, for example, 25% for an aerosol optical thickness of, for example, 1.0 means 0.75 for the boundary layer and 0.25 for the troposphere.)

		AOT at 550 nm		
Model	Humidity (%)	Boundary layer (BL) (0–2 km)	Troposphere (2–12 km)	Stratosphere (12–50 km)
1 2 3 4	70 80 95 99	Maritime* 0.03 0.1 0.3 0.5 1	Continental† Mixing ratio 5% of BL	H_2SO_4† 0.005
5 6 7 8	70 80 95 99	Maritime* 0.03 0.1 0.3 0.5 1	Continental† Mixing ratio 25% of BL	H_2SO_4† 0.005

*Shettle and Fenn (1979); †WCRP (1986).

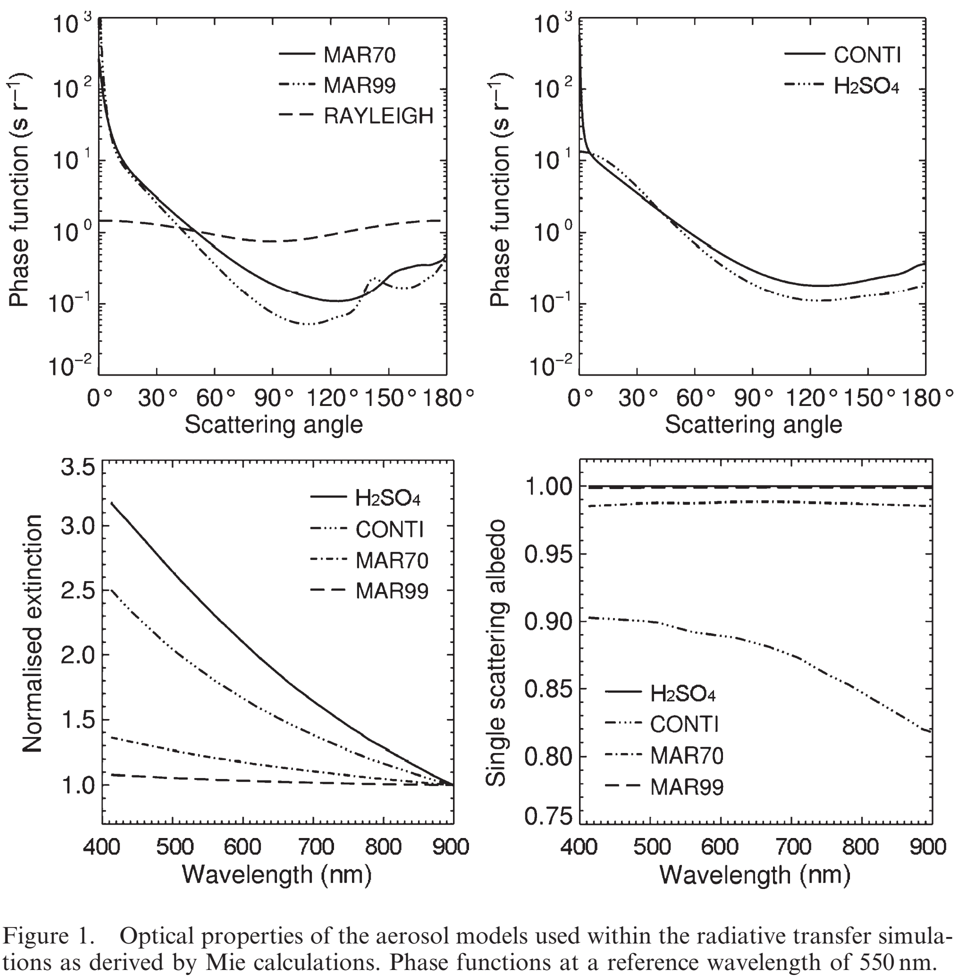

Figure 1. Optical properties of the aerosol models used within the radiative transfer simulations as derived by Mie calculations. Phase functions at a reference wavelength of 550 nm.

particulate matter (a_{p1}) as a function of CHL, plus the absorption of inorganic particulate matter (a_{p2}) as a function of TSM and the absorption of YEL (a_y). The total scattering coefficient (b_{WAT}) of equation (2) was modelled as the sum of pure sea water scattering (b_w) and the scattering of TSM (b_p).

$$a_{WAT} = a_w(\lambda) + a_{p1}(\lambda, \mathrm{CHL}) + a_{p2}(\lambda, \mathrm{TSM}) + a_y(\lambda, \mathrm{YEL}) \tag{1}$$

$$b_{WAT} = b_w(\lambda) + b_p(\lambda, \mathrm{TSM}) \tag{2}$$

The value for a_w was taken from Pope and Fry (1997) and Hale and Querry (1973) while the value for b_w was taken from Morel (1974). We also computed a_{p1} according to Bricaud *et al.* (1998) and a_{p2} was modelled according to the parameterization of Babin (2000). YEL was assumed to be totally absorbing (a_y) and was taken, like b_p, from Babin (2000). The scattering phase function of pure water was taken from Morel (1974). Moreover, a new model of the backscattering probability in case-2 waters was applied from Zhang *et al.* (2002). It relates to the backscattering of marine particles to the wavelength and the ratio of YEL absorption to TSM concentration and was derived by reconciling RT simulations of the hemispherical reflectance just below the sea surface with the corresponding values contained in the COASTLOOC (COAstal Surveillance Through Observation of Ocean Colour) data set (Babin 2000).

2.2 *Inverse model parameterization*

The aim of the present paper was to derive the bottom-of-atmosphere (BOA) remote sensing reflectances (RS_{BOA}) of case-2 waters from remotely sensed data by using extended RT simulations. The most straightforward approach would be the use of the forward model as a look-up table. This look-up table would have the spectral TOA signatures, the observation and illumination geometries and the environmental data (surface pressure, wind speed) as entry data. In turn, each entry would be linked to the corresponding desired output data (here, spectral BOA remote sensing reflectances and spectral AOTs). Thus the task of an atmospheric correction would be to work through this look-up table for a given measurement until the 'best-matching' entry was found. A suitable 'best-matching' criterion is the Euclidian distance. The attached output data would then represent the spectral RS_{BOA} and AOT for the measured spectral TOA signature. This procedure would have to be performed for millions of pixels in a single MERIS scene, which would be very inefficient. A faster retrieval would be possible if the look-up table approach were approximated by a functional relationship in either a parametric (i.e. Chebychev polynomials; Schiller and Doerffer 1993) or non-parametric (i.e. neural networks) approach (Bishop 1995, Schiller and Doerffer 1999). We preferred the latter by using a neural network as a suitable model because it is well known that multilayer feedforward networks with non-linear transfer functions are universal function approximators (Hornik *et al.* 1989). The neural network serving as an inversion model applied here is a fully connected feedforward network. Its free parameters (the so-called weights) are estimated during a supervised learning procedure based on a least mean squares approach; samples pulled randomly from the simulated data set are presented to the network and its output is compared against the expected output as given in the data base. The estimation error, that is the difference between the network's output and the expected output, is used to adapt the parameters of the network. This has to be done sequentially for all data sets until the total estimation error is minimal. In our case we used the backpropagation algorithm (Werbos 1974, Rumelhart and McClelland 1986) to train the network. The network applied here consists of three layers of neurons, an input layer, a hidden layer and an output layer, and is thus able to perform a highly non-linear function approximation (Bishop 1995). While the number of neurons for the input and output layers is fixed by the dimension of the problem under investigation, the optimum number of neurons for the hidden layer has to be optimized by the training of different networks. As there is no theoretical model to simply fix the optimum architecture, it has to be found iteratively by varying the number of neurons in the hidden layer. However, over-fitting occurs if too many neurons are chosen. The network then loses its power of generalization, which results in interpolation deficiencies, and the computation time increases. If too few hidden neurons are used, however, the error function may be minimized poorly (Bishop 1995).

A total of eight different networks with hidden layer neurons varying from 40 to 100 were trained and validated against *in situ* measurements. For the training of the atmospheric correction networks, two subsets of TOA radiance spectra each containing 100 000 training and test vectors were extracted randomly from the simulated database. One input vector consisted of a complete simulated MERIS spectrum (except bands 8, 11, 15), the sun and observing geometry, the surface pressure and the wind speed. We did not use MERIS band 8 (681 nm) because inelastic scattering of chlorophyll fluorescence was not considered in the forward model. Moreover, MERIS band 11 (760 nm) was not taken into account because it is affected by oxygen absorption and MERIS band 15 (900 nm) was not considered because of the influence of water vapour absorption. Signal-dependent Gaussian noise was added to all training vectors according to the assumed uncertainty of the associated parameters and compared to training runs without any additional noise. A principal component analysis (PCA) transformation was used to decorrelate all input dimensions to the network to improve the convergence of the training phase. During the training phase the generalization power of the network was controlled by the test data set not being used for the network training. The output of the atmospheric correction networks is the remote sensing reflectance RS (see equation (3)) at BOA for MERIS bands 1–7 and 9 with additional outputs of the AOT at wavelengths 440, 550, 670 and 870 nm, respectively. The spectral RS is usually defined by the upward radiance L_u depending on the height level z, the solar zenith θ and the azimuth difference ϕ divided by the downward irradiance E_d

$$\mathrm{RS}\,(z,\lambda,\theta,\phi) = L_u(z,\lambda,\theta,\phi)/E_d(z,\lambda) \quad \left(\mathrm{s\,r}^{-1}\right) \tag{3}$$

3. Application to MERIS data

Prior to presenting real MERIS data to the networks, two normalizations have to be applied to be consistent with the simulation framework. First, the TOA radiances need to be normalized to the actual spectral solar constant values contained in the Level1b data file. Second, the TOA radiances have to be normalized to an ozone loading of 344 DU as used for the RT simulations. Therefore, the direct ozone transmission for a 344 DU simulation and for the ozone amount at the time of the MERIS overpass have to be calculated. The total ozone amount at the time of the MERIS measurement was taken from the resampled ECMWF data of the Level1b annotation data set while the spectral ozone extinction coefficients were taken from Baur (1953). After these pre-processing steps we applied the associated Level1b masks, namely LAND/OCEAN to get all the water pixels, the BRIGHT_PIXEL mask mainly to avoid clouds and the GLINT mask to check and reject severe sun glint contributions. Finally, we adapted the PCA rotation to the input vectors.

4. Algorithmic validation

Validation of all atmospheric correction networks is performed by comparing the ANN outputs with coincident *in situ* measurements of the marine reflectance and the spectral AOT.

4.1 *Description of the in situ data set*

The validation data set consists of reflectance spectra measured with the SIMBAD Advanced version (SIMBADA) hand-held field radiometer for 4 days in 2003 on ship cruises performed by GKSS in North Sea turbid waters during Calibration and Validation (CAL/VAL) campaigns for the ENVISAT sensors. Spectral AOTs from CIMEL automatic sun–sky scanning radiometer (sun photometer) measurements of the AERONET station on Helgoland Island and their associated MERIS Level1b data file were available for 12 days of the years 2002 and 2003. The Institute of Coastal Research for GKSS, Geesthacht, Germany operates a CIMEL sun–sky scanning radiometer on Helgoland Island (N 54° 10′, E 7° 53′, altitude 33 m). This island has an area of about 1 km^2 and is located in optically complex case-2 waters at about 70 km off the mainland, in the middle of the German Bight, directly in the region of interest for the MERIS data evaluation. All dates of the *in situ* measurements and their associated MERIS files are presented in table 3.

The CIMEL automatic sun–sky scanning radiometer is suitable for the measurement and retrieval of most aerosol optical properties and operates worldwide in the frame of the AERONET (http://aeronet.gsfc.nasa.gov) and other radiometer networks. Its characteristics, calibration methods and accuracy, and the processing of

Table 3. The validation data set used in this work consisting of *in situ* measured reflectances and aerosol optical thicknesses (AOTs) and their associated MERIS data (if available).

	MERIS data				*In situ* data	
	Level 1b	Level 2	Resolution	Processor	R_{BOA}	AOT
29 July 2002	✓	–	RR	6.3*	–	✓
14 August 2002	✓	–	RR	6.3*	–	✓
3 September 2002	✓	–	RR	6.3*	–	✓
13 April 2003	✓	–	RR	3.55	–	✓
17 April 2003	✓	–	RR	3.55	–	✓
23 April 2003	✓	–	RR	3.55	–	✓
29 April 2003	✓	–	RR	3.55	✓	✓
26 June 2003	✓	–	RR	4.06	–	✓
14 July 2003	✓	–	RR	4.06	–	✓
15 July 2003	✓	✓	RR	4.06	✓	–
5 August 2003	✓	✓	RR	4.06	✓	✓
6 August 2003	✓	✓	FR	4.06	✓	✓
9 August 2003	✓	–	RR	4.06	–	✓

FR, full resolution; RR, reduced resolution.
*MEGS, MEris Ground Segment data processing prototype.

the measured data to get an assured quality data set are described in detail by Holben *et al.* (1998). The automatic sun-pointing requires operation on stationary platforms such as the Helgoland Island station.

The SIMBADA hand-held field radiometer, developed at the University of Science and Technology in Lille, France, operates in the sun-viewing mode for the measurement of the sun extinction and in the sea-viewing mode for the measurement of the water-leaving radiance, providing the AOT and the marine reflectance (Bécu *et al.* 2002). The marine reflectance is measured using a vertical polarizer and a specific geometry (at 45° from nadir and a relative azimuth angle of 135° between the solar plane and the viewing direction) to reduce sun glint and skylight reflection effects, which are crucial for all above-water measurement techniques (Fougnie *et al.* 1999, Deschamps *et al.* 2004). SIMBADA is a compact, light field radiometer with a full field of view (FOV) of 3°, a vertical polarizer, different gains for the sea- and sun-viewing modes, a global positioning system (GPS) antenna and internal memory, which allows its operation from the ship without stopping. Moreover, azimuth, roll and pitch are permanently recorded during the measurements. It belongs to a network of field instruments operating from ships of opportunity.

CIMEL and SIMBADA radiometers were also conceived for the validation of satellite data because they are collimated radiometers with narrow pass-bands centred at the ocean-colour sensor's bands as presented in table 4. They were used during MERIS CAL/VAL campaigns in the German Bight for the measurement of the AOT and the marine reflectance. These two parameters are needed for validation of atmospheric corrections algorithms (Fargion and Mueller 2000, Deschamps *et al.* 2004).

For two reasons, we used the marine reflectance data set from SIMBADA only and preferably used the AOT data set from the CIMEL radiometer. The first is that the inaccuracy of the SIMBADA AOT in the published literature (Holben *et al.* 1998, Deschamps *et al.* 2004, Miller *et al.* 2005) is estimated to be 0.012–0.019, compared to less than 0.01 for AERONET AOT for wavelengths greater than 440 nm. The full-angle FOV is 3° for the SIMBADA and 1.2° for the CIMEL radiometer. The inaccuracy of SIMBADA measured AOT is mainly due to the error of the calibration factor but also to the greater FOV. A larger FOV allows measurement of direct sunlight but also includes light scattered by the atmosphere. This effect increases dramatically for the coarse mode aerosols (desert dust and marine aerosols) with scattering phase functions peaked highly forward (Deschamps *et al.* 2004, Russell *et al.* 2004). Another error could result from the manual sun-pointing from SIMBADA instead of the automatic sun-pointing, which depends on the experience of the operator. The second reason is that the AERONET AOT data set covers 12 days whereas the SIMBADA data set covers only 4 days, and therefore AERONET covers a wider range of atmospheric conditions.

Table 4. Centre wavelengths (nm) of each spectral band related to the ground-based radiometers deployed within the validation campaigns. The bands shown in bold were used in this study.

CIMEL	340	380		**440**		**500**			**670**		**870**
SIMBADA	350	380	**410**	**443**	**490**	**510**	**560**	**620**	**670**	**750**	**870**

4.2 *Validation with in situ reflectance data*

With a knowledge of the geographic location of the *in situ* data through GPS measurements, we were able to relocate and match-up the measured SIMBADA reflectance spectra within the ANN inverted MERIS data files. Based on this, we extracted the median values from 3×3 pixel boxes centred at each *in situ* location. A box size of 3×3 pixels was selected because the absolute geolocation accuracy of the MERIS data is calculated to be around the pixel size of a MERIS full-resolution pixel, which is about 300 m (Colagrande and D'Alba 2004). As outlined in table 3, all MERIS validation data except for one day are available in RR mode with pixel sizes of about 1×1 km at nadir. As a result of the match-up analysis, figure 2 shows the relocated *in situ* stations in the RGB composites of the MERIS data.

Because of heavy tidal effects of the North Sea waters we restricted the comparison to *in situ* reflectance measurements to a maximum time difference of

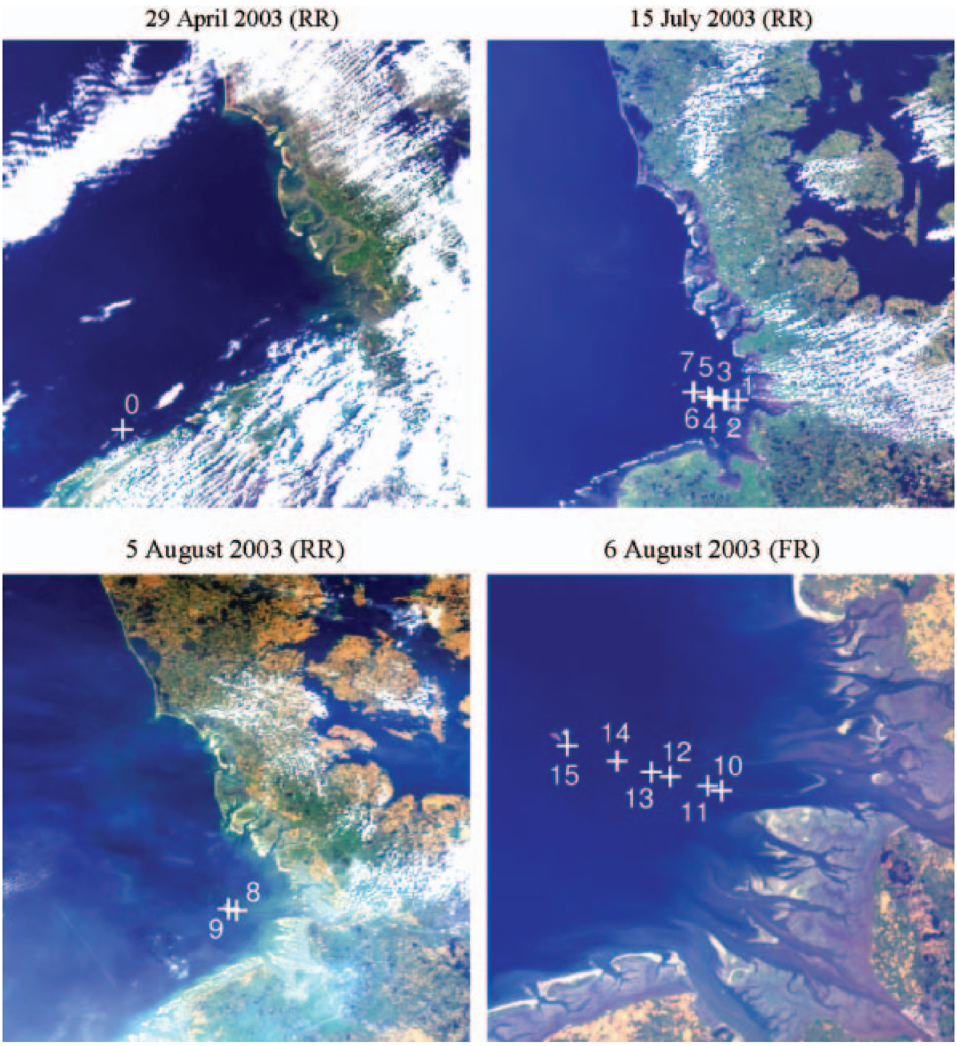

Figure 2. RGB-composites of the MERIS Level1b data files with the relocated stations of the *in situ* reflectance measurements performed by GKSS with the SIMBADA radiometer.

Table 5. Validation results for all neural networks achieved by comparison with the *in situ* data shown in table 3.

Network	Hidden layer neurons	Noise*	RMSE/Correlation	
			RS_{BOA}	AOT
1	40	no	$5.48\times10^{-3}/7.84\times10^{-1}$	$1.05\times10^{-1}/6.29\times10^{-1}$
2	40	yes	$4.84\times10^{-3}/8.97\times10^{-1}$	$1.07\times10^{-1}/8.16\times10^{-1}$
3	60	no	$3.28\times10^{-3}/9.23\times10^{-1}$	$0.81\times10^{-1}/8.11\times10^{-1}$
4	60	yes	$2.94\times10^{-3}/9.45\times10^{-1}$	$0.82\times10^{-1}/8.94\times10^{-1}$
5	80	no	$3.23\times10^{-3}/9.32\times10^{-1}$	$0.89\times10^{-1}/7.38\times10^{-1}$
6	80	yes	$2.75\times10^{-3}/9.38\times10^{-1}$	$0.74\times10^{-1}/7.42\times10^{-1}$
7	100	no	$2.95\times10^{-3}/9.39\times10^{-1}$	$0.82\times10^{-1}/8.13\times10^{-1}$
8	100	yes	$2.82\times10^{-3}/9.37\times10^{-1}$	$0.84\times10^{-1}/8.40\times10^{-1}$

*Signal dependent, uniformly distributed and Gaussian.

$\pm$ 30 minutes to the MERIS overpasses. To remain within the validity range of the bio-optical model, the ranges of the *in situ* spectra were checked against the ranges of the simulated reflectances used to adapt the inverse models to avoid possibly erroneous extrapolations of the networks. All MERIS match-up pixels needed to be flagged as good with no Level1b BRIGHT_PIXEL and GLINT mask applied. We also checked the ranges of all ANN input parameters against the ranges of the simulations. Sixteen *in situ* spectra passed the above criteria and were selected for validation. To compare the SIMBADA reflectance measurements with the ANN retrieved remote sensing reflectances, the ANN spectra need to be multiplied by a factor of π while the SIMBADA spectra are linearly interpolated to match the MERIS wavelengths.

The validation results in terms of the overall root mean square error (RMSE) and the correlation coefficient are outlined for all networks in table 5. Best results were achieved for a network with 80 hidden layer neurons trained on the noisy data set. The left side of figure 3 visualizes the high correlation of 0.94 between the ANN retrieved and the *in situ* measured reflectances as a scatter plot for the MERIS bands 1–7 and 9. The error bars indicate the simple standard deviations within the 3×3

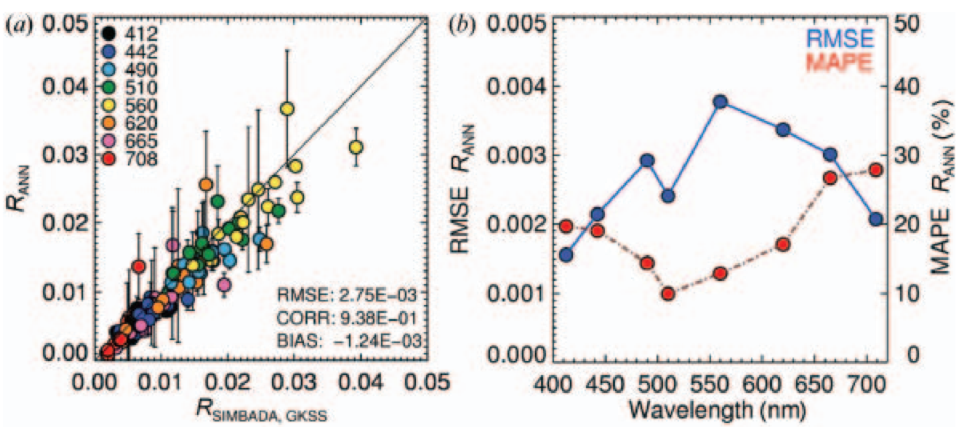

Figure 3. Best results of the reflectance validation achieved by a network with 80 hidden layer neurons through comparison with *in situ* measured spectra as scatter plot (*a*). Spectral RMSE and MAPE (*b*). Total spectra N=16.

pixel boxes. The overall RMSE in reflectance units within the wavelength range 412.5–708.75 nm is 0.0028 with a small BIAS of −0.0013. The spectral slopes of the absolute and relative errors are plotted in figure 3(*b*). For the above-mentioned spectral range the mean absolute percentage error (MAPE) was calculated to be 18%.

4.3 *Comparison with MERIS Level2 data*

Table 3 presents the validation data set of the *in situ* measurements and the availability of the associated MERIS Level2 data files. However, before making any comparison the Product Confidence Flags (PCDs) and the Science Flags of the MERIS Level2 files at the associated *in situ* locations need to be analysed to check the quality of the Level2 pixels. In total, 29 flags are stored in the Level2 products. The PCDs exist for every geophysical parameter and give the user information about the quality of the processing in order to reject bad pixels from further analysis; the products are stored in the data structures even though a specific processing may have failed. Information about special properties or characteristics of a pixel (e.g. glint) is given by the Science Flags (Brockmann 2003*a*).

For a comparison with MERIS Level2 reflectances, the PCD_1_13, MEDI_GLINT and HIGH_GLINT flags needed to be analysed. A comparison is performed only for the case that none of the these flags is raised within the 3×3 pixel boxes. The PCD_1_13 flag will be raised if one of the retrieved surface reflectances is of poor quality; for example, in the case of negative reflectances due to atmospheric correction failure. Both glint flags were checked to avoid sun glint contamination. Although the MERIS Level2 processor corrects for medium glint, which is selected depending on certain thresholds (Montagner and Billat 2000), we rejected all glint flagged pixels from further analysis. The analysis of the glint flags revealed that the Level2 data of 5 August 2003 had to be excluded. For 29 April 2003 no Level2 product was available to us. Finally, 13 spectra remained for a comparison between ANN, MERIS Level2 and *in situ* measured reflectances.

Figure 4 shows the scatter plots of the *in situ* measurements against the median reflectance values derived from the MERIS Level2 product (figure 4(*a*)) and the

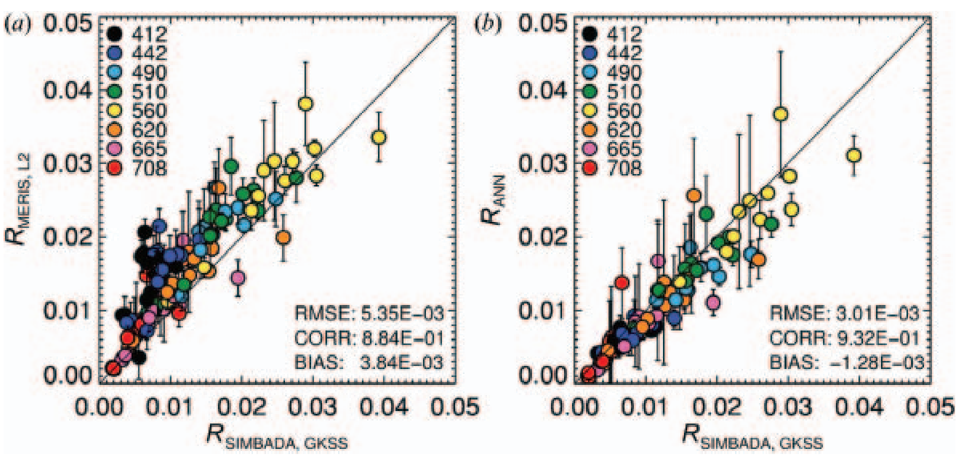

Figure 4. Scatter plots of the median reflectances of the MERIS Level2 product (*a*) and the proposed ANN algorithm (*b*) compared to the *in situ* reflectances measured by GKSS with the SIMBADA radiometer. Total spectra N=13.

values obtained from the ANN (figure 4(*b*)). We found a lower overall RMSE of 0.003 and a higher correlation of 0.93 for the proposed ANN atmospheric correction algorithm compared to the MERIS Level2 product, revealing an overall RMSE of 0.005 and a correlation of 0.88. The spectral error slopes plotted in figure 5 show the largest differences in the blue part of the spectrum, where the MERIS Level2 reflectances result in errors up to 122% compared to 19% for the ANN algorithm. Figure 6 gives an overview of the spectral reflectance comparison at all stations with MERIS Level2 data available. To provide an impression of the glint flagged MERIS Level2 spectra we also plotted the data of 5 August even though these data were excluded from the above error analysis.

4.4 *Validation with in situ AOT data*

As outlined in section 3.2, the presented atmospheric correction networks were provided with additional outputs of the AOT at four wavelengths (440, 550, 670 and 870 nm) for a further validation. Three of these (AOT440, AOT670 and AOT870) match the AERONET wavelengths for a convenient and direct comparison. An output at 550 nm was selected because this is the AOT reference wavelength of the RT simulations. As presented in table 3, *in situ* AERONET data from Helgoland Island are available for 12 days of the years 2002 and 2003. The AOT data are of Level2 quality in version 1, which means the data are cloud screened. The atmospheric composition was assumed not to change as rapidly as the composition of the turbid North Sea water. Therefore a time window of $\pm$ 60 minutes to the MERIS overpass was allowed to compare the median of the ANN-retrieved AOTs with the median values of the sun photometer measurements. The AERONET data were linearly interpolated to 550 nm. The validation boxes were centred at Helgoland Island with box sizes of 20×20 pixels for the RR data and 80×80 for the FR case. Prior to the inversion the MERIS Level1b LAND/OCEAN, BRIGHT_PIXEL and GLINT masks were checked. Again, best results were achieved by the network with 80 hidden layer neurons (see table 5). Figure 7 shows the scatter plot of the ANN

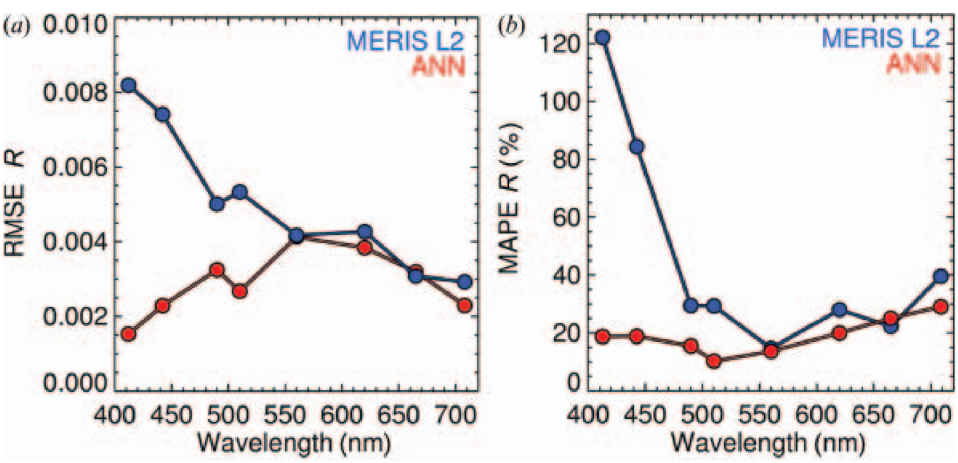

Figure 5. By comparison with *in situ* measured reflectances derived spectral slopes of the RMSE (*a*) and MAPE (*b*) for the MERIS Level2 product (blue) and the proposed ANN algorithm (red).

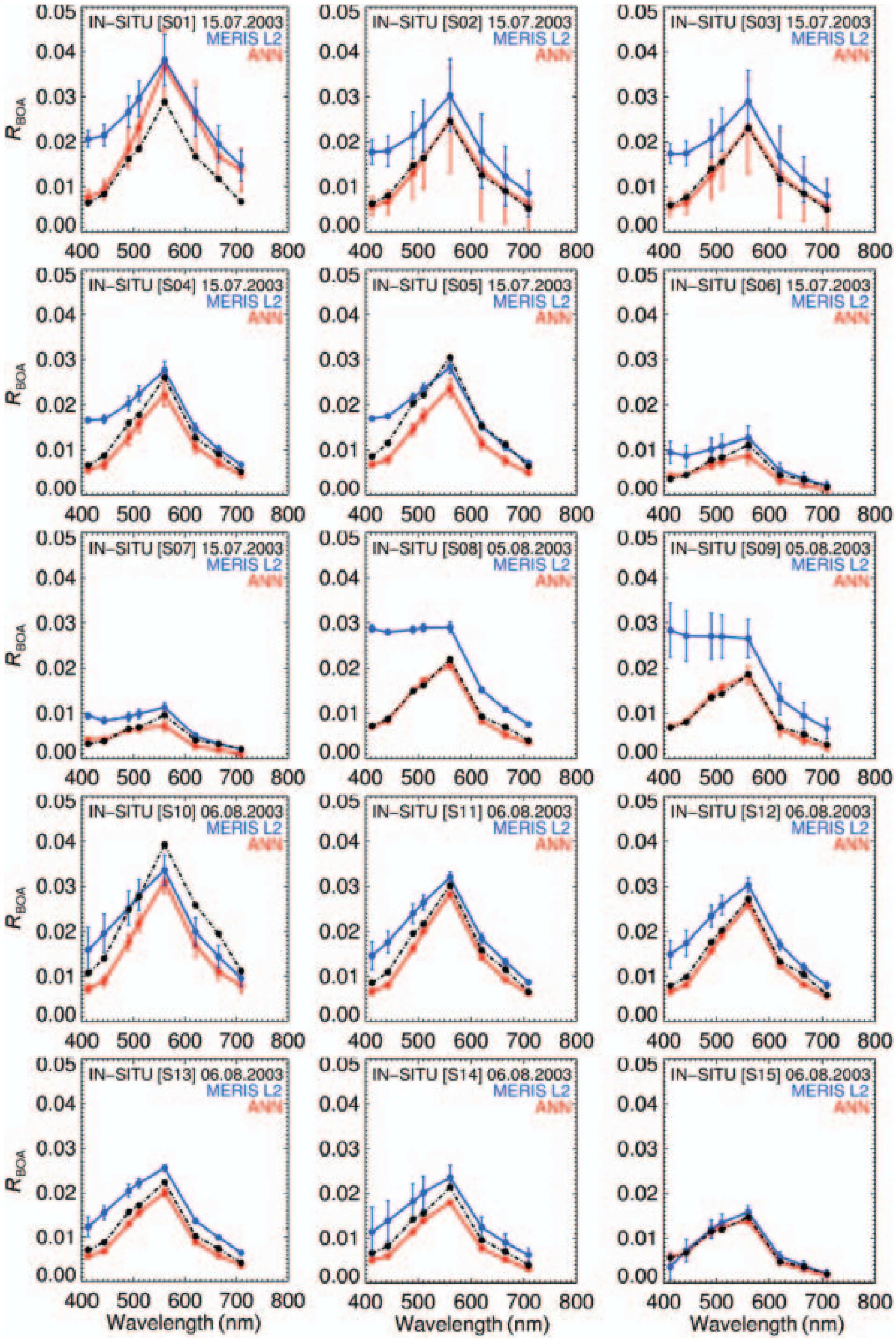

Figure 6. Spectral reflectances as derived by the proposed atmospheric correction algorithm (red) compared to the *in situ* measurements (black) and to the standard MERIS Level2 product (blue). The station numbers (S01–15) correspond to the *in situ* locations shown in figure 2.

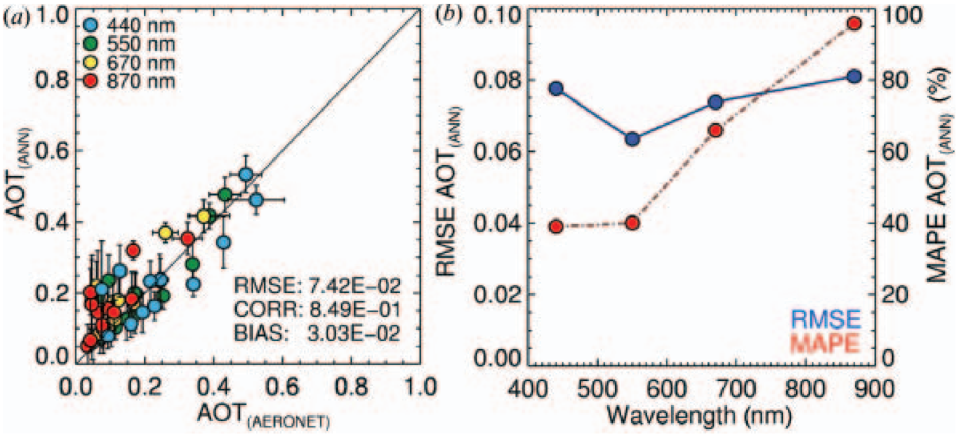

Figure 7. Best results of the aerosol optical thickness (AOT) validation achieved by a network with 80 hidden layer neurons through comparison with *in situ* measured AOT spectra from the AERONET station on Helgoland Island as a scatter plot (*a*). Spectral slopes of RMSE and MAPE (*b*). Total spectra $N=12$.

inverted data against the *in situ* measured data. The overall RMSE in AOT units was calculated as 0.074 with a small BIAS of 0.003 and a high correlation of 0.84. The training of the networks as described above consists of minimizing an absolute error for all training vectors. Therefore, the spectral error slopes in figure 7 show a more constant absolute error, while the mean absolute relative error is lowest in the blue part of the spectra (40%), because of the relatively high AOTs, and highest in the NIR (96%) because of the relatively low AOTs in this spectral region.

To illustrate the performance of the proposed atmospheric correction algorithm, figure 8 shows maps of the derived spatial reflectance and AOT distribution as derived from a MERIS reduced resolution scene acquired on 15 July 2005 covering parts of the North and Baltic Sea regions. The derived structures reveal that no features from the water body are visible in the AOT product and therefore a good separation of atmospheric and oceanic parameters has been obtained. The reflectance maps plotted for wavelengths 442 and 560 nm show the expected structures due to the typical distribution of the water constituents. High TSM concentrations in the North Sea coastal regions cause high reflectances values at 560 nm and lower ones at 442 nm, whereas the off-shore regions of the North Sea waters show higher reflectance values at 442 nm compared to 560 nm because these areas are associated with clear water. In contrast to the North Sea coastal areas the coastline of the Baltic Sea, as shown in figure 8, stays uninfluenced by strong tidal effects, resulting in lower reflectances at 560 nm due to the assumed lower TSM concentrations.

5. Summary and conclusions

An atmospheric correction algorithm for MERIS data above case-2 waters has been presented that derives the remote sensing reflectance and the AOT from the TOA measured radiances. The algorithm was validated with a set of *in situ* reflectance and AOT data. For the reflectance product a mean absolute percentage error of 18% within the spectral range of 412.5–708.75 nm could be derived while the RMSE of the AOT was found to be 0.074 within the spectral range of 440–870 nm. Compared

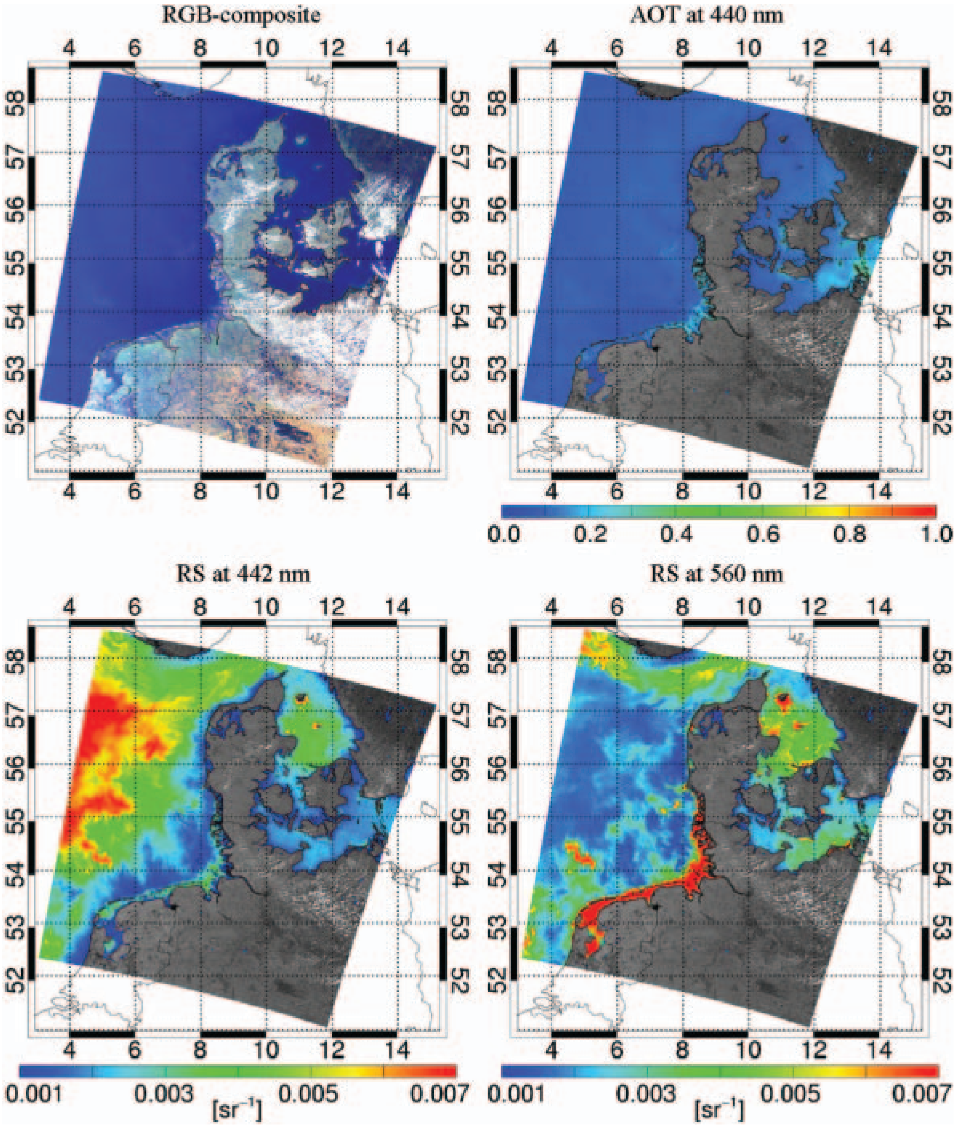

Figure 8. Example maps of the derived spatial remote sensing reflectance at 442 and 556 nm and the AOT distribution at 440 nm as derived from a MERIS reduced resolution scene acquired on 15 July 2005 covering parts of the North and Baltic Sea regions.

to the standard MERIS Level2 reflectance product of the processor versions 3.55 and 4.06, the proposed algorithm reveals a significant improvement in accuracy, especially in the blue part of the spectrum.

The atmospheric algorithm outlined in this paper is available to the broad ocean colour community in the form of a Plug-in for the Basic ERS and ENVISAT (A)ATSR and MERIS Toolbox (BEAM) (Brockmann, 2003*b*) and can be obtained free from the official BEAM website (BEAM 2005). Within the BEAM environment a more sophisticated cloud masking can be applied to the Level1b data in running an integrated cloud probability processor instead of using the Level1b

BRIGHT_PIXEL flag. Although the BRIGHT_PIXEL flag does not account for thin cirrus or subpixel clouds, absolutely clear-sky conditions were assured in this work from additional observations during *in situ* sampling.

Acknowledgements

We thank G. Bécu and P. Y. Deschamps from the Laboratoire d'Optique Atmospherique in Lille, France, for providing the calibration and retrieval of the SIMBADA reflectance data. Thanks to Peter Kipp, Institute for Coastal Research, GKSS, for establishing and maintaining the Helgoland AERONET site. We also thank the AERONET staff for the data collection, processing and calibration. We are grateful to all participants of the CAL/VAL campaigns from the Institute for Coastal Research, GKSS. This work was funded by the European Commission under contract number EVG1CT2000-00034 (NAOC, Neural Network Algorithms for Ocean Color).

References

Babin, M., 2000, *COAstal Surveillance Through Observation of Ocean Colour (COAST-LOOC)*, Final Report, Project ENV4-CT96-0310. Laboratoire de Physique et Chimie Marines, Villefranche-sur-mer, France.

Baur, F. (Ed.), 1953, *Linkes Meteorologisches Taschenbuch, Band 2* (Leipzig: Akademische Verlagsgesellschaft Geest & Porting).

BEAM 2005, Available online at: www.brockmann-consult.de/beam/plugins.html (accessed 15 December 2005).

Bécu, G., Deschamps, P.Y. and Nicolas, J.M., 2002, MERIS Level-2 products validation using SIMBADA radiometer network. In *ENVISAT Validation Workshop Proceedings*, ESA ESRIN, Frascati, Italy, published on CD-Rom, ESA SP-531.

Bishop, C.M., 1995, *Neural Networks for Pattern Recognition* (New York: Oxford University Press).

Bricaud, A., Morel, A., Babin, M., Allali, K. and Claustre, H., 1998, Variations of light absorption by suspended particles with chlorophyll *a* concentration in oceanic (case 1) waters: analysis and implications for bio-optical models. *Journal of Geophysical Research*, **103**, pp. 31 033–31 044.

Brockmann, C., 2003a, Scope of water products – the quality and science flags. In *Proceedings of the MERIS User Workshop*, ESA ESRIN, Frascati, Italy, published on CD-Rom, ESA SP-549.

Brockmann, C., 2003b, Demonstration of the BEAM software – a tutorial for making best use of VISAT. In *Proceedings of the MERIS User Workshop*, ESA ESRIN, Frascati, Italy, published on CD-Rom, ESA SP-549.

Colagrande, P. and D'Alba, L., 2004, *MERIS Cyclic Report 24*, ESA document. Available online at: http://earth.esa.int/pcs/envisat/meris/reports (accessed 15 December 2005).

Cox, M. and Munk, W., 1954, Measurements of the roughness of the sea surface from photographs of the sun's glitter. *Journal of the Optical Society of America*, **44**, pp. 838–850.

Deschamps, P.Y., Fougnie, B., Frouin, R., Lecomte, P. and Verwaerde, C., 2004, SIMBAD: an advanced field radiometer to measure aerosol optical thickness and marine reflectance. *Applied Optics*, **43**, pp. 4055–4069.

Doerffer, R. and Fischer, J., 1994, Concentrations of chlorophyll, suspended matter, and gelbstoff in case II waters derived from satellite coastal zone color scanner data with inverse modeling methods. *Journal of Geophysical Research*, **99**, pp. 7457–7466.

Fargion, G.S., and Mueller, J.L. (Eds), 2000, *Ocean Optics Protocols for Satellite Ocean Color Sensor Validation: Revision 2*, NASA Tech. Memo 2000-209966 (Greenbelt, MD: NASA Goddard Space Flight Center).

FISCHER, J. and GRASSL, H., 1984, Radiative transfer in an atmosphere–ocean system: an azimuthally dependent matrix operator approach. *Applied Optics*, **23**, pp. 1032–1039.

FELL, F. and FISCHER, J., 2001, Numerical simulation of the light field in the atmosphere–ocean system using the matrix operator method. *Journal of Quantitative Spectroscopy and Radiative Transfer*, **69**, pp. 351–388.

FOUGNIE, B., FROUIN, R., LECOMTE, P. and DESCHAMPS, P.Y., 1999, Reduction of skylight reflection effects in the above-water measurement of diffuse marine reflectance. *Applied Optics*, **38**, pp. 3844–3856.

HALE, G.M. and QUERRY, M.R., 1973, Optical constants of water in the 200 nm to 200 mm wavelength region. *Applied Optics*, **12**, pp. 555–563.

HOLBEN, B.N., ECK, T.F., SLUTSKER, I., TANRE, D., BUIS, J.P., SETZER, A., VERMOTE, E., REAGAN, J.A., KAUFMAN, Y., NAKAJIMA, T., LAVENU, F., IANKOWIAK, I. and SMIRNOV, A., 1998, AERONET – a federated instrument network and data archive for aerosol characterization. *Remote Sensing of Environment*, **66**, pp. 1–16.

HORNIK, K., STINCHCOMBE, M. and WHITE, H., 1989, Multilayer feed-forward networks are universal approximators. *Neural Networks*, **2**, pp. 359–366.

JAMET, C., MOULIN, C. and THIRIA, S., 2004, Monitoring aerosol optical properties over the Mediterranean from SeaWiFS images using a neural network inversion. *Geophysical Research Letters*, **31**, p. L13107.

LAND, P.E. and HAIGH, J.D., 1996, Atmospheric correction over case 2 waters with an iterative fitting algorithm. *Applied Optics*, **35**, pp. 5443–5451.

MILLER, M., KNOBELSPIESSE, K., FROUIN, R., BARTHOLOMEW, M., REYNOLDS, R., PIETRAS, C., FARGION, G., QUINN, P. and THIEULEUX, F., 2005, Analysis of shipboard aerosol optical thickness measurements from multiple sun photometers aboard the R/V Ronald H. Brown during the Aerosol Characterization Experiment – Asia. *Applied Optics*, **44**, pp. 3805–3820.

MONTAGNER, F. and BILLAT, V., 2000, *Sun Glint Flag Algorithm*, ESA document ATBD 2.13, Doc. no. PO-TN-MEL-GS-0005, ACRI. Available online at: http://envisat.esa.int/instruments/meris/data-app/level2.html (accessed 8 October 2006).

MOREL, M., 1974, Optical properties of pure water and sea water. In *Optical Aspects of Oceanography*, N.G. Jerlov, and E. Steemann Nielsen (Eds), pp. 1–24 (New York: Academic Press).

MOREL, M. and PRIEUR, L., 1977, Analysis of variations in ocean color. *Limnology and Oceanography*, **22**, pp. 709–722.

NOAA, NASA and USAF 1976, *U.S. Standard Atmosphere*, Technical Report NOAA-S/T 76-1562 (Washington DC: U.S. Government Printing Office).

POPE, R. and FRY, E.S., 1997, Absorption spectrum (380–700 nm) of pure water. II. Integrating cavity measurements. *Applied Optics*, **36**, pp. 8710–8723.

RAST, M., 1999, The ESA Medium Resolution Imaging Spectrometer MERIS – a review of the instrument and its mission. *International Journal of Remote Sensing*, **20**, pp. 1679–1680.

RUMELHART, D. and MCCLELLAND, J., 1986, *Parallel Distributed Processing* (Cambridge, MA: MIT Press).

RUSSELL, P.B., LIVINGSTON, J.M., DUBOVIK, O., RAMIREZ, S.A., WANG, J., REDEMANN, J., SCHMID, B., BOX, M. and HOLBEN, B.N., 2004, Sunlight transmission through desert dust and marine aerosols: diffuse light corrections to Sun photometry and pyrheliometry. *Journal of Geophysical Research*, **109**, D08207, doi:10.1029/2003JD004292.

SCHILLER, H. and DOERFFER, R., 1993, Fast computational scheme for inverse modeling of multispectral radiances: application for remote sensing of the ocean. *Applied Optics*, **32**, pp. 3280–3285.

SCHILLER, H. and DOERFFER, R., 1999, Neural network for emulation of an inverse model operational derivation of case II water properties. *International Journal of Remote Sensing*, **9**, pp. 1735–1746.

SCHROEDER, TH., 2005, Fernerkundung von Wasserinhaltsstoffen in Küstengewässern mit MERIS unter Anwendung expliziter und impliziter Atmosphärenkorrekturverfahren. Doctoral Thesis, Freie Universität Berlin. Available online at: www.diss.fu-berlin.de/2005/78/ (accessed 15 December 2005).

SHETTLE, E.P. and FENN, R.W., 1979, Models for the aerosols of the lower atmosphere and the effects of humidity variations on their optical properties. *Environmental Research Papers*, No. 676, AFGL-TR-79-0214, USAF.

WCRP 1986, *World Climate Research Program: A Preliminary Cloudless Standard Atmosphere for Radiation Computation*, International Association of Meteorology and Atmospheric Physics, Radiation Commission, WCP 112.

WERBOS, P.J., 1974, Beyond regression: new tools for prediction and analysis in the behavioral sciences. Doctoral thesis, Harvard University, MA, USA.

ZHANG, T., FELL, F. and FISCHER, J., 2002, Modeling the backscattering ratio of marine particles in case-2 waters. In *Proceedings of the Ocean Optics XVI*, Santa Fe, USA, published on CDROM.

ZHANG, T., 2003, Retrieval of oceanic constituents with artificial neural network based on radiative transfer simulation techniques. Doctoral thesis, Freie Universität Berlin.